DOI https: //doi. org/10.1007/s11595-020-2257-x

Corrosion Behavior of Plasma Transferred Arc Fe-based Coating Reinforced by Spherical Tungsten Carbide in Hydrochloric Acid Solutions

DONG Yaohua[1,3], FAN Li[2*], CHEN Haiyan[1], DONG Lihua[1], YIN Yansheng[1], SUN Fanghong[3]

(1.College of Ocean Science and Engineering, Shanghai Maritime University, Shanghai 201306, China; 2. College of Mechanical and Electronic Engineering, Shanghai Jian Qiao University, Shanghai 201306, China; 3. School of Mechanical Engineering, Shanghai Jiaotong University, Shanghai 200240, China)

Abstract: Fe-based coatings reinforced by spherical tungsten carbide were deposited on 304 stainless steel using plasma transferred arc (PTA) technology. The composition and phase microstructure of the coatings were evaluated using scanning electron microscopy (SEM), energy dispersive spectrometer (EDS) and X-ray diffraction (XRD). The corrosion behaviors of the coatings in 0.5 mol/L HCl solution were studied using polarization curve and electrochemical impedance spectroscopy (EIS) measurements. The experimental results shows that the tungsten carbide improves the corrosion resistance of the Fe-based alloy coating, but increase in the mass fraction of tungsten carbide leads to increasing amount of defects of holes and cracks, which results in an adverse effect on the corrosion resistance. The defects are mainly present on the tungsten carbide but also extend to the Fe-based matrix. The tungsten carbide, acting as a cathode, and binding material of Fe-based alloy, acting as an anode, create a galvanic corrosion cell. The binding material is preferentially corroded and causes the degradation of the coating.

Key words: plasma transferred arc (PTA); spherical tungsten carbide; Fe-based alloys; corrosion resistance; electrochemical impedance spectroscopy

1 Introduction

It is well known that 304 stainless steel (304SS) has good mechanical properties and chemical corrosion resistance. However, its low hardness and poor wear resistance restricts its application as a key moving part in an equipment due to friction[1-3]. In order to enhance the wear resistance of the 304 stainless steel, the Fe-based alloy coating reinforced by spherical tungsten carbide has been employed using plasma transferred arc (PTA) technology[4]. The coating showed relatively high hardness and excellent wear resistance in a series of hardness, friction and wear tests. However, in the practical circumstances, it is inevitable that the coating would be in direct contact with a variety of highly corrosive media which may potentially degrade its performance due to corrosion.

Previous research[5] has shown that cemented carbide coatings are generally multi-phase materials, and the Co bonding material and WC hard phase could form a galvanic corrosion cell. As a result, their corrosion is basically electrochemical in nature. In general, the standard reduction potential of a tungsten carbide hard phase is higher than that of the bonding phase which tends to act as an anode and corrode, while the hard phase, acting as a cathode, is less affected. Hochstrasser *et al*[6] studied the corrosion behavior of a WC-Co cemented carbide coating in corrosive solutions at various pH values and demonstrated that the corrosion of coating in acidic or neutral corrosive media was dominated by the

corrosive dissolution of the Co bonding phase with a small amount of dissolution of the WC phase. However, in alkaline solution, the Co bonding phase was passivated, whilst the solubility of WC phase was significantly increased. The galvanic corrosion between Co and WC due to potential differences accelerated the corrosion rate of the Co bonding material and reduced the dissolution of the WC hard phase. Furthermore, the

(Received: May 15, 2019; Accepted: July 18, 2019)

DONG Yaohua(董耀华): Assoc.Prof.; E-mail: yhdong@shmtu.edu.cn

*Corresponding author: FAN Li(范丽): E-mail: 635164479@qq.com

Funded by the China Postdoctoral Science Foundation (No.2017M620153) and the Science & Technology Program of Shanghai Jian Qiao University (No.SJQ19012)

galvanic corrosion occurred in the corrosive medium of all pH values. The studies carried out by Bozzini *et al*[7] have revealed that the hard alloy coatings have good corrosion resistance in neutral corrosion solutions at room temperature, but were severely corroded in strong acidic solutions. Therefore, the improvement of the corrosion resistance of the alloy coatings reinforced by tungsten carbide is of great scientific value and practical significance.

In this work, the Fe-based coatings reinforced by spherical tungsten carbide were deposited on the surface of 304 stainless steel using PTA technology. Their corrosion behavior was investigated in 0.5 mol/L HCl solution.

2 Experimental

2.1 Materials

The 304 stainless steel (304SS) was used as the matrix material. The Fe-based powder and tungsten carbide powder used for PTA is manufactured by Hoganas Co. Ltd (Netherlands). The powders are spherical with particle size ranging from 45 to 150 μm. Their chemical composition, apparent density, and other parameters are provided by the manufacturer, as presented in Table 1. The powder without tungsten carbide is labeled as Fe, and the powders mixed with 30% and 60% mass of tungsten carbide are designated as Fe+30%WC and Fe+60%WC, respectively.

2.2 Fabrication of the coating

The Fe-based powder used for PTA was mixed with the tungsten carbide powder in accordance with the proportions of 30% and 60%. Then the combined powders were further mixed in the QM-3SP4 planetary ball mill for 2 h and baked in an oven for 1 h to increase the fluidity and prevent them from blocking the powder feeding tube. The Fe-based coating reinforced by spherical tungsten carbide was deposited using PTA-PHE equipment (Saint-Gobain, France). The deposition parameters are shown in Table 2.

2.3 Microstructural characterization

The samples with dimension of 10 mm×10 mm × 8 mm were machined by use of wiring cutting, and characterized using metallographic, X-ray diffraction (XRD) and electrochemical testing. And the coated samples with the size of 5 mm× 5 mm× 2 mm were used for immersion test.

The surface and cross-section of the metallographic observation specimens were successively ground to 2 000 grit size by SiC paper and polished to a mirror surface with 1.5 μm Al_2O_3, etched with aqua regia (HNO_3:HCl=1:3). JSM 7500F SEM was used to observe the combination of substrate and coating as well as the structure of coating. The X-ray energy spectrum analysis (EDS) was used to help judge the element composition of the microstructure.

The surface of coated specimens for XRD testing was ground to 400 grit size by SiC paper. Coating phase analysis was conducted on PANalytical X' Pert PRO XRD with Cu Kα rays, the working voltage and current were 40 kV and 10 mA, respectively, and in a scanning range of 2θ from 20° to 80°.

2.4 Electrochemical corrosion test

As the reference material, corrosion tests were also carried out on the 304 stainless steel substrate. Prior to electrochemical corrosion test, the specimens were sealed with expoxy resin with a working electrode area of 1 cm^2 was left. Thereafter, electrode surface was ground with successive grades of SiC water-proof abrasive paper up to 2000 grit, polished and ultrasonically cleaned with ethanol, and dried. The electrochemical corrosion tests were performed at room temperature, in 0.5 mol/L solution using the Autolab PGSTAT 302N type electrochemical working station. A three electrode system was used. A standard saturated calomel electrode (SCE) was served as the reference electrode and the auxiliary was platinum wire.

After immersion in open circuit potential for 60 min to make its corrosion potential basically stable, then the polarization curve was conducted. The scanning rate was 2 mV/s and the scanning range was −1.0-1.5 V, measured by polarization curve. The frequency range tested by EIS test was 10^{-2}-10^5 Hz, and the loading voltage was sinusoidal ac voltage with the volt-

Table 1 Chemical composition, apparent density and hardness of the Fe-based powder and spherical tungsten carbide

Material	Chemical composition /wt%	Apparent density/(g/cm^3)
Fe-based powder	1.76 C; 4.5 Mo; 16.5 Ni; 27.5 Cr; 1.39 Si; 0.73 Mn; Fe bal.	4.4
Spherical tungsten carbide	3.9-4.1 C; W bal.	9.5

Table 2 PTA deposition parameters

Current /A	Voltage /V	Feed rate/(g/min)	Speed/(mm/min)	Vibration extent /mm
130	30	10	50	20

age amplitude of 10 mV. Collecting the EIS data with computer and using Zsimpwin software to analyze the impedance.

2.5 Immersion test

The Fe, Fe+30%WC, and Fe+60%WC samples were immersed in 0.5 mol/L HCl for 3 d and then cleaned with deionized water before being air-dried. The surface corrosion morphology of the above dried samples was observed with JSM 7500F SEM. XPS test was performed on ESCALAB 250Xi surface analyzer (Thermo Fisher Scientific Company) with monochrome Al target (1486.6 eV) as the X-ray source.

3 Results and discussion

3.1 Microstructure and phase analysis

Fig.1 shows the XRD spectra of the three tested Fe-based PTA coatings. The diffraction calibration peaks indicate that the Fe coating is mainly composed of γ-Fe, FeNi, and Cr_7C_3, while the phase of the Fe-based coating reinforced by spherical tungsten carbide is more complex and has additional phases such as WC, W_2C, Fe_6W_6C, and Mo_2C.

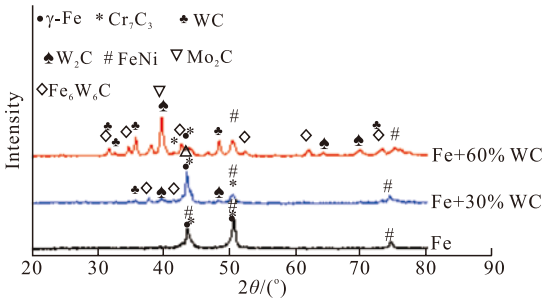

Fig.1 XRD patterns of PTA coatings

The SEM micrograph of the Fe surface layer in Fig.2(a) shows that the PTA coating is composed of massive austenite dendrites (Region A), and lamellar eutectic structures (Region B). According to the EDS results in Fig.2(b), Region A is rich in Fe and Ni, while Region B in Fig.2(c) is rich in Cr, C, and Mo. Combined with XRD phase analysis, it can be seen that the large area contains γ-Fe with a face-centered cubic (fcc) structure and a solid solution of FeNi with a large amount of Ni. The eutectic structure is composed of an intermetallic compound M_7C_3 (M = Cr or Mo) and γ-Fe. The hard phase M_7C_3 is mainly composed of Cr and Mo and is distributed in the eutectic structure formed by austenite rich in Cr. There is also a small amount of Cr and Mo in the austenite dendrites, which can be attributed to the fact that Cr and Mo elements are completely soluble in Fe atoms during cooling and solidification, which forms a solid solution rich in Cr and Mo.

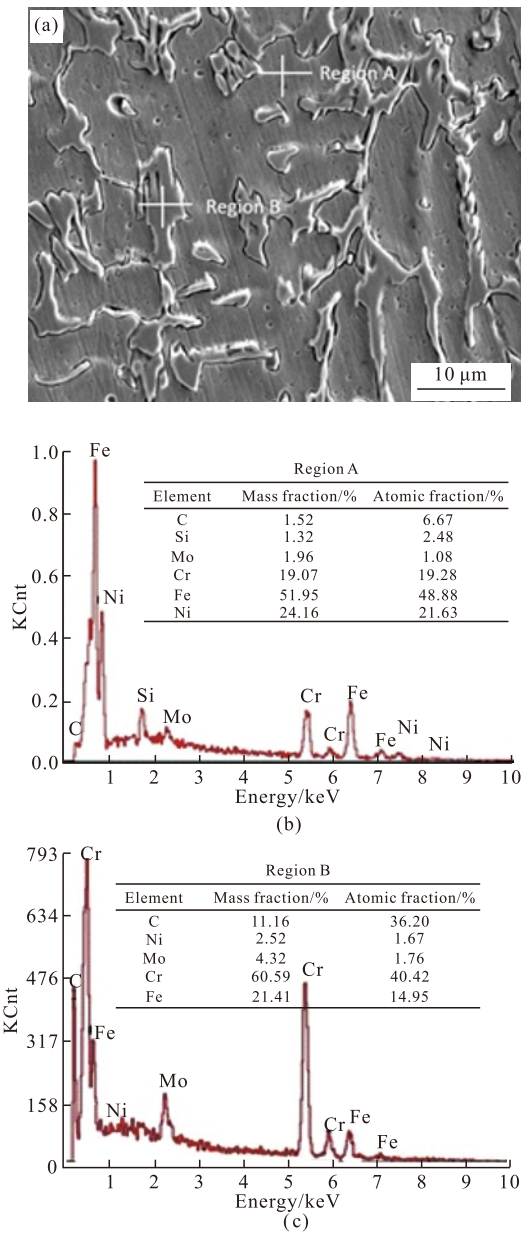

Fig.2 Microstructure of Fe PTA coating (a); (b) EDS spectrum of Region A marked in (a); and (c) EDS spectrum of Region B marked in (a)

Fig.3 shows the SEM images of the Fe-based PTA coatings reinforced with spherical tungsten carbide. Compared to the pure Fe-based coating, new components appear in the Fe+30%WC and Fe+60%WC coatings, such as coarse herringbone carbides, block precipitation, and spherical reinforced tungsten carbide particles embedded in the Fe-based matrix. Combined with the previous XRD results[8,9], it can be shown that coarse herringbone carbides are Fe_6W_6C, and the block precipitation is Mo_2C.

Fig.4 shows the cross-sectional SEM images of PTA Fe-based coating reinforced by spherical tungsten

carbide. The coating thickness is about 500-600 μm, and a metallurgical combination formed between the coating and the substrate [10].

Fig.5 shows the surface and cross-sectional SEM images in BSE mode of Fe-based coatings reinforced by spherical tungsten carbide. There are some cracks, holes, and other defects on the surface and cross-sections of the Fe-based coating reinforced with spherical tungsten carbide. The cracks are mainly concentrated on tungsten carbide and tend to expand into the Fe-based matrix. Compared to the Fe+30%WC coating, the Fe+60%WC coating has both larger and more cracks.

As the content of tungsten carbide increases, small holes and other defects in the coating tend to increase. The main reasons are that the melting point of the tungsten carbide is as high as 2 870 ℃, and only a small percentage of tungsten carbide particles are melted at high temperatures, and the vast majority of them remain spherically-shaped during the PTA process. Since the content of tungsten carbide is low, the liquid Fe-based alloy can be completely coated on the surface of tungsten carbide to form a compact composite coating. However, as the tungsten carbide content increases, the liquid Fe-based alloy cannot quickly wet the entire surface of tungsten carbide and fill all its pores. Therefore, as the content of tungsten carbide increases, the number of small holes and other defects in the coating increases[11].

Previous literature reports on PTA matrix-based coatings reinforced by spherical tungsten have attributed the causes of tungsten carbide cracks to the fact that the thermal expansion coefficient of tungsten carbide is lower than the binder phase matrix material[12]. There-

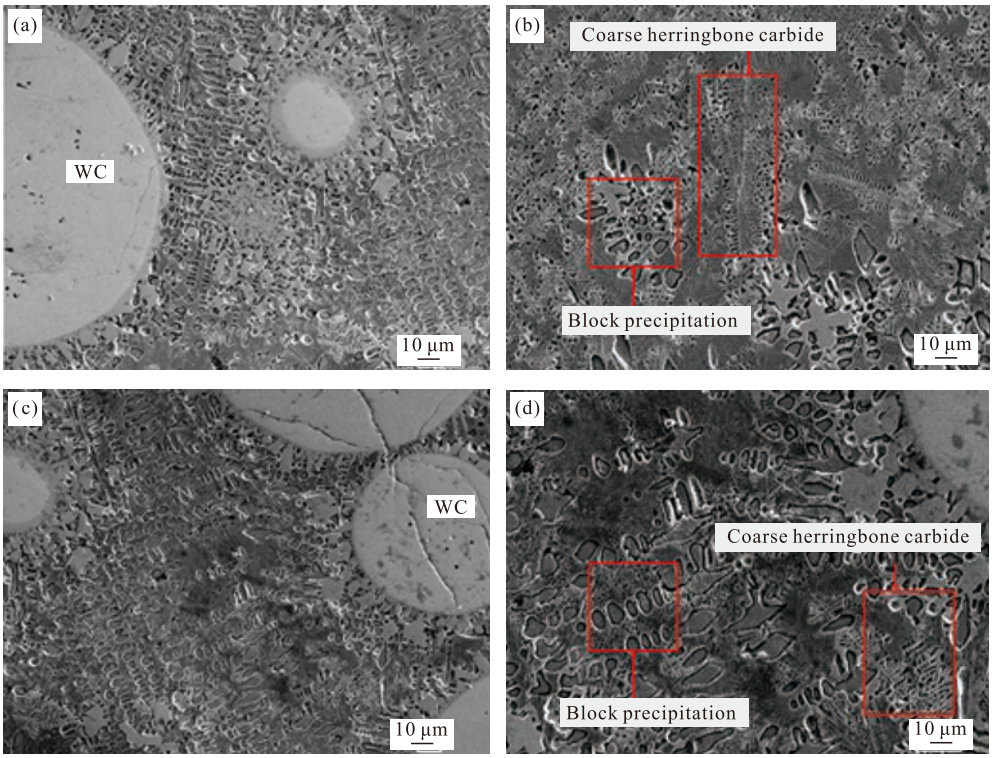

Fig.3 Low (a, c) and high (b, d) magnified SEM images of Fe/WC composite coatings: (a, b) Fe + 30%WC coating and (c, d) Fe + 60% WC coating

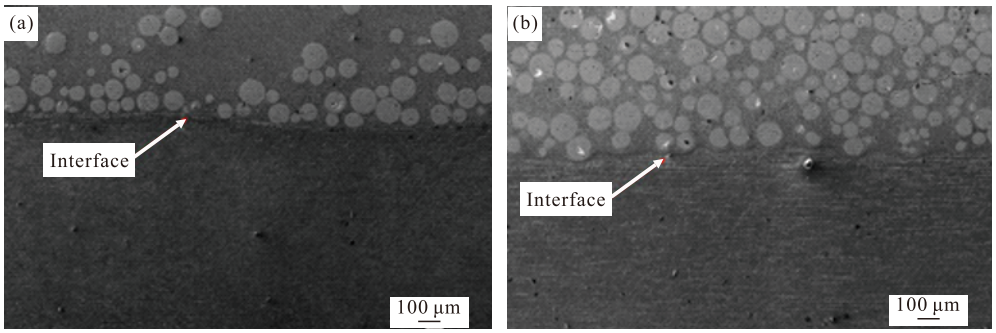

Fig.4 Cross-sectional SEM images of Fe/WC coatings: (a) Fe+30%WC and (b) Fe+60%WC

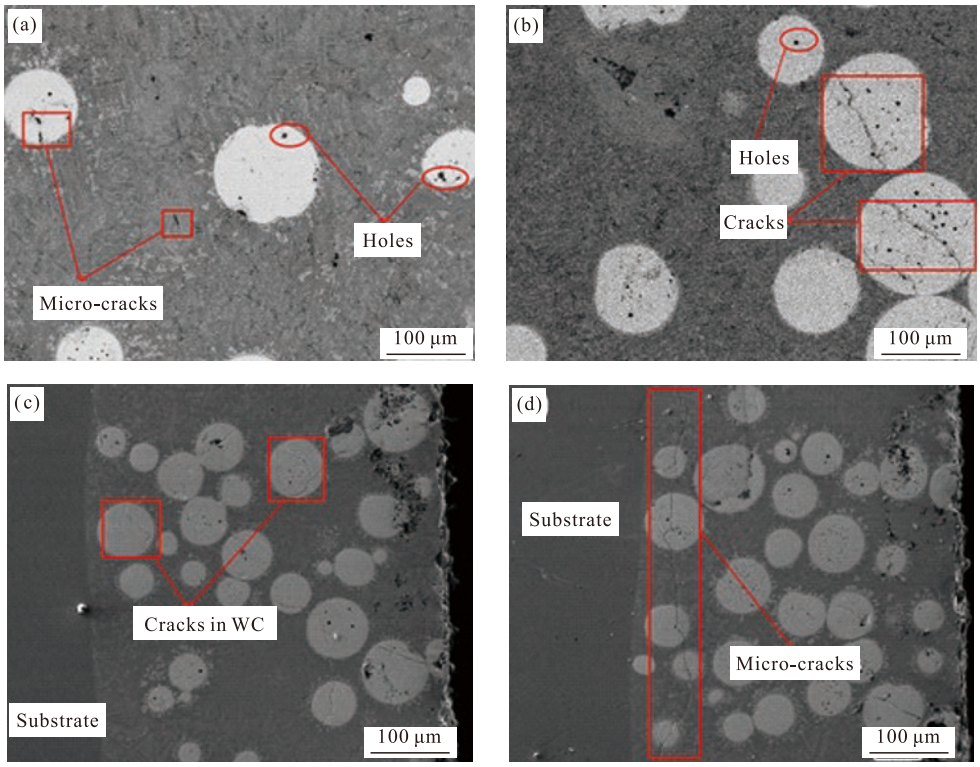

Fig.5 (a, b) Surface and (c, d) cross-sectional SEM images in BSE mode of Fe/WC composite coatings: (a, c) Fe+30%WC coating and (b, d) Fe+60%WC coating

fore, when thermal stresses produced during the PTA process exceed the yield strength of tungsten carbide, micro-cracks initiate in weaker portions of tungsten carbide particles and ultimately extend through the tungsten carbide particles. The thermal stress of a PTA coating can be calculated according to Eq. (1):

$$\sigma_{th} = E \times \Delta\alpha \times \Delta T / (1 - \nu) \quad (1)$$

where, E is the Young's modulus of the coating, υ is the Poisson's ratio of the coating, $\Delta\alpha$ is the difference between the thermal expansion coefficient of the coating and matrix, and ΔT is the difference between the coating temperature and room temperature.

Tungsten carbide has a low thermal expansion coefficient, and as the content of tungsten carbide particles in Fe/WC composite powder increase, the thermal expansion coefficient of the surface layer decreases. In addition, the deposition of tungsten carbide particles due to the high density during the PTA leads to uneven thermal expansion coefficients in different coating areas[13-15]. The bottom area of the coating has more tungsten carbide particle sedimentation, and the $\Delta\alpha$ value is higher because of its low thermal expansion coefficient. According to Eq.(1), the thermal stress in this area of the coating is the highest, and the tungsten carbide particles in this area also have the largest cracking tendency. In contrast, on the coating surface with a lower tungsten carbide particle distribution, there are fewer cracks and pores because the thermal expansion coefficient of the surface material is relatively high and the thermal stress is relatively low.

3.2 Potentiodynamic polarization results

Fig.6 shows the potentiodynamic polarization curves of the Fe-based PTA coating and 304SS in 0.5 mol/L HCl solution. These polarization curves are composed of active solution, activation and passivation transformation, stable passivation, and over-passivation zones. In HCl solution, the possible electrochemical reactions of coating components are shown in Eqs.(2)-(6):

$$2H^+ + 2e^- \rightarrow H_2 \quad (2)$$

$$Ni - 2e^- \rightarrow Ni^{2+} \quad (3)$$

$$Fe - 3e^- \rightarrow Fe^{3+} \quad (4)$$

$$Cr - 3e^- \rightarrow Cr^{3+} \quad (5)$$

$$WC + 5H_2O \rightarrow WO_3 + CO_2 + 10H^+ + 10e^- \quad (6)$$

According to the Ref.[16], when active dissolution occurs in acidic solutions, the Fe potential in coatings was the lowest, as shown in Fig.7, and Fe dissolved first. As the degree of dissolution increased, both the corrosion potential and the corrosion current density

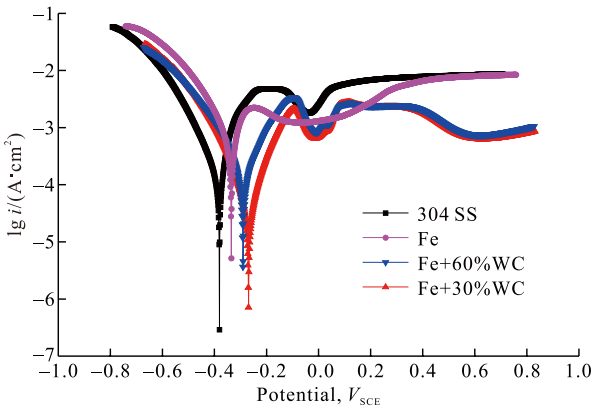

Fig.6 Potentiodynamic polarization curves of Fe/ tungsten carbide PAT coatings and 304SS

also increased. However, when the reaction was in the stable passivation zone, the corrosion current density remained stable as the corrosion potential increased. This indicated that the passivation that occurred on the surface of the material during the polarization process prevented further corrosion of the coating. At potentials higher than the highest potential in the stable passivation zone, the current increased once again, the passivation was damaged, and the corrosion intensified. Corrosion products remaining on the interface impeded additional diffusion of the corrosion solution into the coating, which caused a phenomenon similar to passivation.

Compared to 304SS and the pure Fe-based PTA coatings, there are two passivation zones in the coating reinforced by tungsten carbide. After surpassing the first passivation zone, the current density continued to increase with a positive potential and entered the second passivation zone when the potential was scanned to 0.4 V. The second passivation zone exists because after the Fe-based bonding phase was corroded, tungsten carbide particles came into contact with the corrosive medium, to form a layer of WO_3 oxidation product passivation film that was uniformly attached to the alloy surface[17], which slowed down the corrosion rate. The WO_3 passivation film was thin, and once the passivation potential surpassed or broke the electrode potential, the passivation film was destroyed, and the sample surface once again came into contact with the corrosion solution. As a result, the current density rose sharply, causing decreasing and increasing trends in the current density in the potentiodynamic polarization curve, namely the second passivation stage, which is consistent with the results in the Ref.[18].

The Ref.[19] showed that galvanic corrosion can occur in corrosive media at any pH value, which means it can easily occur between the adjacent binder Fe phase and the hard phase tungsten carbide in an HCl solution. In other words, during the corrosion process, the anodic polarization dissolution occurs in the Fe-based binder phase, and the corrosion rate increases. The hard phase of tungsten carbide polarizes the cathode, which slows the corrosion rate and protects the cathode. In the HCl solution, generated oxides tend to react with acids and dissolve in HCl. Compared to W, iron oxides are more likely to dissolve in HCl, while the undissolved WO_3 loosely attaches to the alloy coating surface, which provides the surface with a relatively low amount of protection from corrosion.

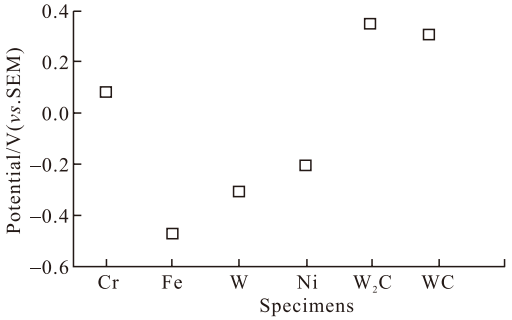

Fig.7 Comparison of the open circuit potential of the constituents of coating materials and substrate in an acidic environment[16]

Therefore, for coatings reinforced by tungsten carbide in HCl solution, during the initial stage of the anodic polarization curve, the increase in current density is due to the dissolution of the binder phase (Fe). At higher electrode potentials, the increase in current density occurs because the hard phase (tungsten carbide) dissolves.

Table 3 shows the results of the corrosion parameter fitting, including the self-corrosion current density i_{corr}, self-corrosion potential E_{corr}, polarization resistance R_p, and Tafel plot slope β_a/β_c. From the perspective of thermodynamics, the self-corrosion potential E_{corr} re-

Table 3 Corrosion parameters fitting results according to the potentiodynamic polarization curves in 0.5 mol/L HCl solution

Material	E_{corr}/mV	i_{corr}/(μA·cm^{-2})	R_p/Ω	β_a/(mV/dec)	β_c/(mV/dec)
Fe-based coating	−314.06	23.08	888.2	123.34	75.59
Fe+30%WC coating	−259.14	8.52	2867.2	142.07	93.17
Fe+60%WC coating	−263.04	10.45	1964.5	125.72	76.67
304SS	−380.68	112.73	113.16	87.57	44.20

flects the tendency of the alloy coating to undergo electrochemical corrosion. The larger this value is, the less it tends to corrode. The self-corrosion current density i_{corr} represents the corrosion rate of the material from the perspective of dynamics. Generally, materials that have smaller i_{corr} values have better corrosion resistances.

As can be seen from Fig.6 and Table 3, the cathodic polarization curves of Fe-based PTA coating samples with different tungsten carbide contents have similar shapes while the β_a slope values of the anode Tafel plot show significant differences. The order of the change is Fe+30%WC > Fe+60%WC > Fe. In addition, the β_a slope values of the anode Tafel plot of the three groups of PTA samples are all greater than those of the cathode Tafel slope. Analysis of the Evans diagram of corrosion polarization, the anode process resistance is greater than the cathode process, and the corrosion process is mainly controlled by the anode process. A large amount of Cl^- in HCl solution is absorbed on the surface of the alloy coating, which affects the depolarization of H^+ in the cathode and the active dissolution process of the alloy anode. Therefore, it can be determined that the corrosion rate of the Fe-based PTA coating in HCl solution is controlled by the anode, and a larger anode area results in a larger Cl^- adsorption area. This also increases the dissolution rate of the anode.

According to the polarization curve fitting results shown in Table 3, a comparison of E_{corr} values shows that the lowest value of 304SS is −380.68 mV. Compared to this value, the self-corrosion potential of the pure Fe-based coating samples and the coating samples reinforced by tungsten carbide samples were improved by different degrees. The self-corrosion potential of the coating samples with 30%WC content were the highest at −259.14 mV. However, as the tungsten carbide content increases to 60%WC, the E_{corr} value slightly decreases. The above analysis shows that tungsten carbide help improve the corrosion resistance of the Fe-based alloy coating, but increasing the tungsten carbide content also increases the number of holes, cracks, and other defects in the sample coating, which reduces its corrosion resistance. Therefore, in the tested samples, Fe+30%WC coated samples with less tungsten carbide had the best corrosion resistance.

3.3 EIS results

Fig.8 shows the electrochemical impedance spectra (EIS) and equivalent circuits of the Fe-based PTA coating and 304 stainless steel in 0.5 mol/L HCl solution. According to Nyquist plots in Fig.8(a), the impedance spectra of Fe+30%WC and Fe+60%WC coatings in 0.5 mol/L HCl solution contained a high-frequency capacitive reactance arc and a low-frequency inductive reactance arc. The high-frequency capacitive reactance arc is closely-related to the electron transfer process on the sample surface, while the low-frequency inductive reactance arc is mainly caused by the adsorption of corrosion products on the sample surface[20].

However, in the impedance spectra of the pure Fe-based coating and 304SS in acidic solution, there is no

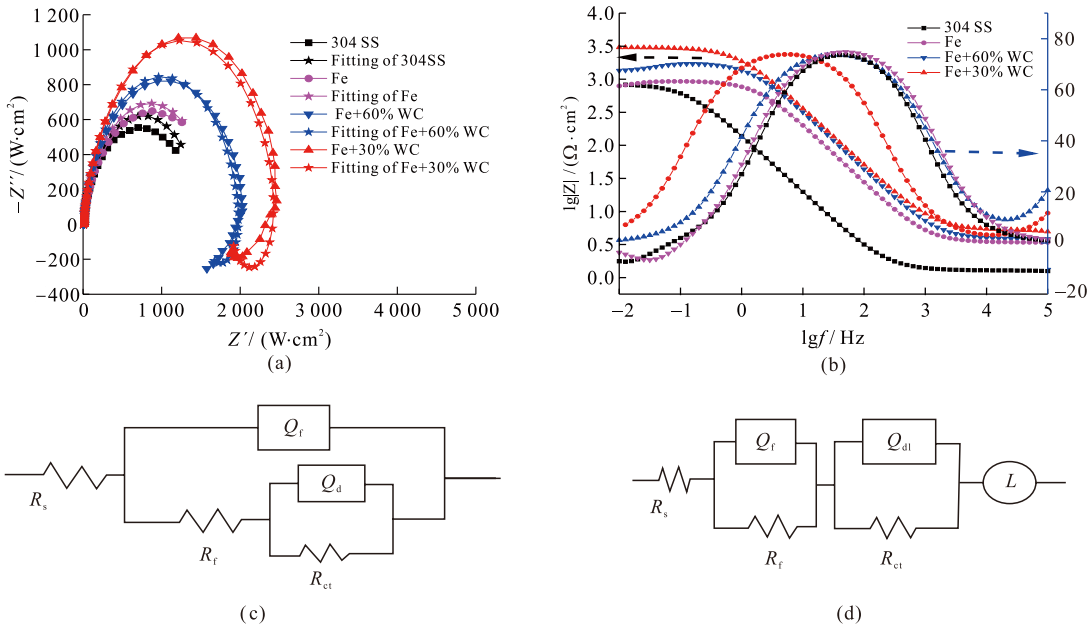

Fig.8 (a) Nyquist plots; (b) Bode impedance plots of different alloys in 0.5 mol/L HCl solution; (c) equivalent circuit of EIS for pure Fe PAT coating and 304SS; and (d) equivalent circuit of EIS for Fe/WC coatings

low-frequency inductive reactance arc, but rather a distorted arc, which is composed of a low-frequency capacitive reactance arc and a high-frequency capacitive reactance arc. The presence of the capacitive reactance arc at low and high frequency capacitive reactance arcs suggests that there are passivation films on the surfaces of the pure Fe-based coating and 304SS electrodes. There are two capacitive impedances during the electrode process: one is the low-frequency capacitive reactance of the passive film itself, while the other is the high-frequency capacitive reactance that corresponds to electrical double-layer capacitors formed on the surface of the passivation film. Therefore, for the Fe-based coating, two-phase angular peaks should appear in its Bode diagram, and as shown in Fig.8(b), the capacitive reactance arc of Fe+30%WC coating is the largest among the four groups of tested samples. The larger the arc radius is, the greater the total impedance of the sample will be. Therefore, the Fe+30%WC coating has a better coating resistance.

In the Bode diagram in Fig.8(b), the impedance value $|Z|$ in the low-frequency region (0.01 - 1 Hz) represents the impedance of the corrosion reaction, and the impedance of the Fe-based coating is higher than 304SS $|Z|$ in the low-frequency region. This suggests that it is more difficult for corrosive ions in HCl solution to affect the substrate through the passive film on the surface of the Fe-based coating. The impedance of Fe+30%WC $|Z|$ is the highest of the three groups of plasma surfacing coatings, indicating that the passivation film more strongly protected the substrate in 0.5 mol/L HCl solution.

The R(Q(R(QR)) equivalent circuit in Fig.8(c) was used to fit the EIS of the pure Fe-based plasma surface coating and 304SS. The LR(QR)(QR) equivalent circuit in Fig.8(d) was used to fit the EIS data of the PTA Fe-based coating reinforced by spherical tungsten carbide. The fitting results are shown in Table 4 and Table 5. R_s represents the resistance of the solution, R_f represents the resistance of the passivation film, Q_f represents the capacitive reactance of the passivation film, Q_{dl} represents the double-layer capacitance formed on the surface of the sample, R_{ct} represents the electrochemical transfer resistance, and L represents the inductive reactance. The EIS equivalent circuit diagram is closely related to the alloy corrosion process, and the complexity of the equivalent circuit can excellently reflect the complexity of the alloy corrosion mechanism. A comparison of the EIS equivalent circuits, shows that the equivalent circuits of the pure Fe-based PTA coating and 304 stainless steel are slightly simpler, and their corrosion mechanisms in HCl should be basically the same. The corresponding equivalent circuits of Fe+30%WC and Fe+60%WC coatings show the inductive reactance behavior due to the attached corrosion products to the surfaces.

According to the data in Table 4 and Table 5, the electrochemical transfer resistance R_{ct} of the three tested PTA coatings are higher than the the 304 stainless steel by about 1.10 times (Fe coating), 1.96 times (Fe+60%WC coating), and 2.54 times (Fe+30%WC coating). Higher R_{ct} values indicate better corrosion resistance, therefore, compared to 304 stainless steel, the Fe-based PTA coating has a lower corrosion rate and higher corrosion resistance in HCl solution, which is consistent with the polarization curve data. Compared to 304 stainless steel, the R_f of the Fe-based PTA coating increases, indicating that the passivation film dissolution rate of the Fe-based PTA coating is less than that of 304SS, and the passivation film more strongly protects the substrate. Comparing the dispersion coefficient n_f in Table 4 and Table 5, show that the n_f of the Fe-based PTA coating is larger, and the passivation film is close to the pure capacitance. This indicates that the passivation film is denser and more strongly protects the metal under the film[21].

3.4 Results of immersion corrosion test

Fig.9 shows the SEM micrographs of the corro-

Table 4 EIS fitting results of pure Fe-based PTA coating and 304SS in 0.5 mol/L HCl solution

Samples	R_s/(Ω·cm^2)	Q_f		R_f/(Ω·cm^2)	Q_{dl}		R_{ct}/(Ω·cm^2)
		Y_0/(Ω^{-1}·cm^{-2}·s^n)	n_f		Y_0/(Ω^{-1}·cm^{-2}·s^n)	n_{dl}	
Fe coating	2.438	4.24×10^{-5}	1	434.2	2.11×10^{-4}	0.9264	519.7
304SS	2.452	2.16×10^{-4}	0.9113	361.2	5.79×10^{-3}	1	473.2

Table5 EIS fitting results of Fe/WC coatings in 0.5 mol/L HCl solution

Samples	R_s/(Ω·cm^2)	Q_f		R_f/(Ω·cm^2)	Q_{dl}		R_{ct}/(Ω·cm^2)	L/(H·cm^{-2})
		Y_0/(Ω^{-1}·cm^{-2}·s^n)	n_f		Y_0/(Ω^{-1}·cm^{-2}·s^n)	n_{dl}		
Fe+30%WC	1.966	3.94×10^{-5}	0.9859	694.7	1.28×10^{-4}	0.9876	1203.6	252.8
Fe+60%WC	1.452	2.96×10^{-5}	0.9768	506.7	5.79×10^{-4}	0.9925	929.5	134.9

sion morphology of the Fe-based PTA coating after being immersed in 0.5 mol/L HCl solution for 3 days. Figs.9 (a, b) show that there are a number of pits on the surface of the Fe-based surface coating after corrosion. According to the failure mechanism of the passivation layer, the pitting appears due to the following reasons: in HCl solution, Cl^- tends to attach to the surface of the passivation film because of its small ionic radius, which increases the electric field intensity of the passivation film, and makes some of the passivation layer to ionically conducting. At this point, the passivation film shows a high current density and makes Mn^+ active. When the electric field intensity of the passivation-solution interface reaches a certain critical value, pitting nucleation occurs, and the dissolution in this area is accelerated. This causes the metal matrix to be deeply eroded downward, forming pits. In corrosion holes with certain occlusion, the dissolved concentration of Mn^+ continues to increase, and to balance the charge, Cl^- keeps entering the pits, leading to Cl^- enrichment, which intensifies the corrosion and expands the pitting. In addition, due to the PTA process characteristics, a certain number of small holes and cracks appear inside the coating, as well as the interface between layers. In these areas the "short circuit effect" is prone to occur, which will accelerate the corrosion, forming larger holes, which provide a channel for the corrosive media to penetrate the material, accelerating the coating corrosion.

Comparing Figs. 9(c, d, e, f), significant corrosion pits, cracks, and pores also appeared on the surface of the Fe-based coating reinforced by tungsten carbide, and the corrosion occurred in the binder phase. In the field of view, some Fe-based binder phases around the tungsten carbide reinforcing phase were detached due to severe corrosion, forming large corrosion holes. Many literatures[20,21] have shown that the preferential dissolution of the binder phase is the main cause of corrosion and failure of the metal matrix coating (MMC) reinforced by tungsten carbide. In HCl solution, the coating surface easily adsorbs Cl^- and electrochemical corrosion occurs, and there is a potential difference

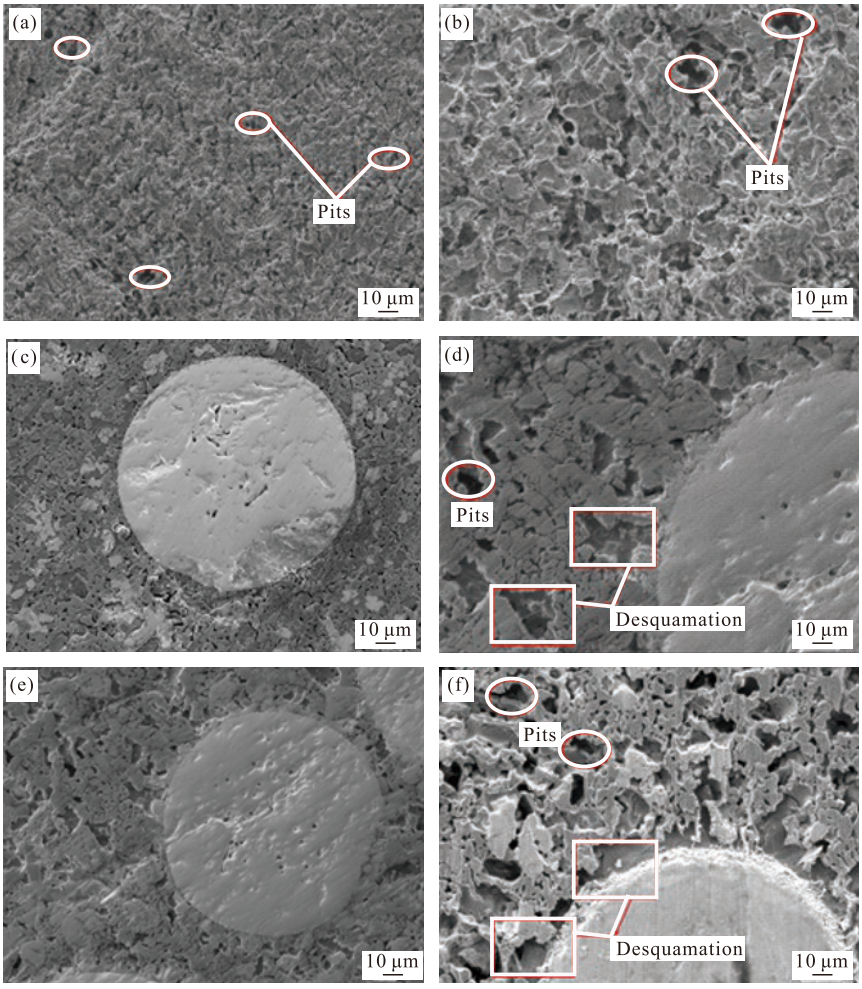

Fig.9 Low (a, c, e) and high (b, d, f) magnified surface corrosion micrograph of Fe-based PTA coatings exposed to 0.5 mol/L HCl solution for 3 d: (a, b) pure Fe-based coating, (c, d) Fe+30%WC coating, and (e, f) Fe+60%WC coating

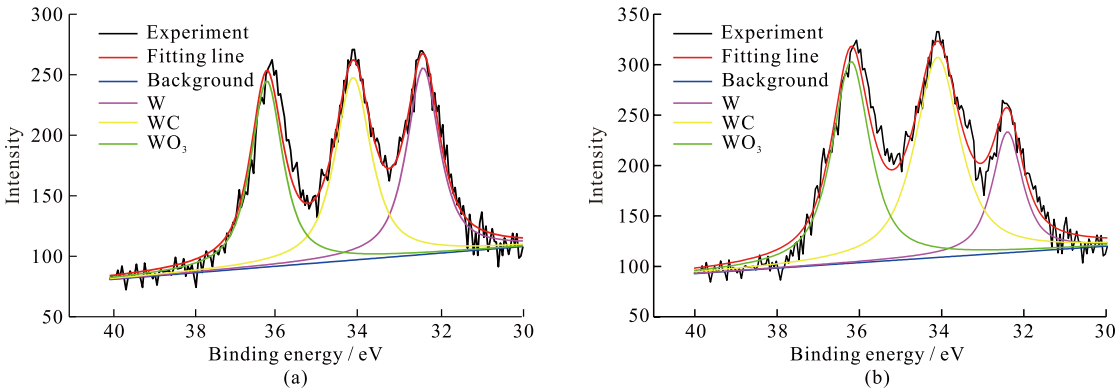

Fig.10 Detailed XPS spectra of W for spherical tungsten carbide reinforced coatings exposed to 0.5 mol/L HCl solution for 3 days: (a) Fe+30%WC coating, and (b) Fe+60%WC coating

between the Fe binder phase and the tungsten carbide hard phase. Electric couple corrosion occurs under the applied voltage and current. The low corrosion potential of Fe leads to the preferential corrosion of the Fe binder phase, especially the Fe phase at the interface of tungsten carbide particles. The desquamations in Figs.9(c, d, e, f) formed when the Fe phase dissolved to a certain extent and fell off.

Pores, cracks, and laminar structures are all important factors that affect the corrosion resistance of the tungsten carbide PTA coating. Coating corrosion generally begins at the surface pores, cracks, and other defects and grows along the interface between tungsten carbide particles or obvious weak areas with laminar structures. The presence of micro-cracks provides a path for the corrosion solution to penetrate, and Cl^- in the HCl solution will accumulate in pores and cracks, causing local pitting corrosion.

As can be seen from Figs.9(c, d, e, f), a higher tungsten carbide content results in more severe corrosion because tungsten carbide has good conductivity, which can form a galvanic battery with the Fe binder phase. The tungsten carbide density is twice as high as the Fe powder, so tungsten carbide sinks to the bottom during the PTA process. At low tungsten carbide content, less tungsten carbide is present on the coating surface, so there are only a small number of galvanic cells, and there is only slight. As the tungsten carbide increases, the tungsten carbide content on the surface of 60%WC coating increases, and the number of corroded galvanic cells also increases, resulting in relatively serious corrosion. Secondly, increasing the tungsten carbide coating decreases the surface quality because of more holes and cracks which allows corrosive ions to easily enter the internal coating through holes, increasing the contact area of the coating and corrosion solution. Further increasing corrosive ions in the holes speed up the corrosion of the deep areas of holes and the entire coating. Thirdly, as the tungsten carbide increases, the thermal expansion coefficient of the coating decreases, which affects gas removal during the heating of surfacing welding, thus resulting in the decreasing compactness of the coating. Therefore, in 0.5 mol/L HCl solution, the corrosion resistance of the surface coating reinforced by tungsten carbide decreases as the tungsten carbide content increases.

The polarization curve and EIS results showed that the corrosion resistance of Fe-based PTA coating samples reinforced by tungsten carbide in HCl solution are superior to the pure Fe-based coating. Previous literature attributed this to the passivation layer, oxidation products of WO_3, that are present on the surface of the alloy coating which slightly slows the corrosion rate. To verify the presence of WO_3, Fe-based PTA coatings reinforced by tungsten carbide in 0.5 mol/L HCl solution for 3 days were tested by X-ray photoelectron spectroscopy (XPS), and then the passive film composition on the surface of the coating was analyzed.

Fig.10 shows detailed XPS spectra of W after the sample with Fe-based PTA layer reinforced by tungsten carbide was exposed to HCl solution for 3 days. It can be seen that the passivation film of WO_3 oxidation product does exist in the corrosion products of the HCl solution.

4 Conclusions

The pure Fe-based PTA coating is mainly composed of γ-Fe, FeNi, and Cr_7C_3, while Fe-based coating reinforced by spherical tungsten carbide is more complex than the pure Fe-based surfacing layer, with more phases such as WC, W_2C, Fe_6W_6C, and Mo_2C.

Some defects, such as cracks and holes, appear on the surface and cross-sections of Fe-based coatings

reinforced by tungsten carbide. The cracks are mainly concentrated on the tungsten carbide and tend to expand to the Fe-based matrix. The bottom layer which has more deposits of tungsten carbide show a high tendency of cracks.

Tungsten carbide helps improve the corrosion resistance of the Fe-based alloy coating, but increasing the mass fraction of tungsten carbide leads to more holes, cracks, and other defects, which has an adverse effect on the corrosion resistance. Therefore, the Fe+30%WC coated sample with lower tungsten carbide content showed the best corrosion resistance.

In HCl solution, the corrosion of the coating reinforced by tungsten carbide showed preferential selective corrosion of the Fe binder phase, while the galvanic corrosion between tungsten carbide and the binder phase was the main cause of corrosion dissolution of the coating.

References

[1] Xu P, Lin CX, Zhou CY, *et al*. Wear and Corrosion Resistance of Laser Cladding AISI 304 Stainless Steel/Al_2O_3 CompositeCoatings[J]. *Surf. Coat. Technol*., 2014, 238(2): 9-14

[2] Lu XL, Liu XB, Yu PC, *et al*. Effects of Heat Treatment on Microstructure and Mechanical Properties of Ni60/h-BN Self-lubricating Anti-wear Composite Coatings on 304 Stainless Steel by Laser Cladding[J]. *Appl. Surf. Sci*., 2015, 355: 350-358

[3] Sun GF, Zhang YK, Zhang MK, *et al*. Microstructure and Corrosion Characteristics of 304 Stainless Steel Laser-Alloyed with Cr-CrB_2[J]. *Appl. Surf. Sci*., 2014, 295: 94-107

[4] Fan L, Dong YH, Chen HY, *et al*. Wear Properties of Plasma Transferred Arc Fe-based Coatings Reinforced by Spherical WC Particles[J]. *J. Wuhan Univ. Technol.-Mater. Sci. Ed*., 2019, 34(2): 433-439

[5] Liu SS, Chen HY, Zhao X *et al*. Corrosion Behavior of Ni-based Coating Containing Spherical Tungsten Carbides in Hydrochloric Acid Solution[J]. *J. Iron Steel Res. Int*., 2019, 26(2): 191-199

[6] Hochstrasser S, Mueller Y, Latkoczy C, *et al*. Analytical Characterization of the Corrosion Mechanisms of WC-Co by Electrochemical Methods and Inductively Coupled Plasma Mass Spectroscopy[J]. *Corros. Sci*., 2007, 49(4): 2 002-2 020

[7] Bozzini B, Gaudenzi GPD, Serra M, *et al*. Corrosion Behaviour of WC-Co Based Hardmetal in Neutral Chloride and Acid Sulphate Media[J]. *Mater. Corros*., 2002, 53(5): 328-334

[8] Zhou SF, Dai XQ. Microstructure Evolution of Fe-based WC Composite Coating Prepared by Laser Induction Hybrid Rapid Cladding[J]. *Appl. Surf. Sci*., 2010, 256: 7 395-7 399

[9] Zhou SF, Dai XQ, Zheng HZ. Microstructure and Wear Resistance of Fe-based WC Coating by Multi-track Overlapping Laser Induction Hybrid Rapid Cladding[J]. *Opt. Laser Technol*., 2012, 44(1): 190-197

[10] Huang Z, Hou Q, Ping W. Microstructure and Properties of Cr_3C_2-modified Nickel-based Alloy Coating Deposited by Plasma Transferred Arc Process[J]. *Surf. Coat. Technol*., 2008, 202(13): 2 993-2 999

[11] Wang J, Li L, Tao W. Crack Initiation and Propagation Behavior of WC particles Reinforced Fe-based Metal Matrix Composite Produced by Laser Melting Deposition[J]. *Opt. Laser Technol*., 2016, 82: 170-182

[12] Huang Y, Zeng X. Investigation on Cracking Behavior of Ni-based Coating by Laser-induction Hybrid Cladding[J]. *Appl. Surf. Sci*., 2010, 256(20): 5 985-5 992

[13] Wu P, Du HM, Chen XL, *et al*. Influence of WC Particle Behavior on the Wear Resistance Properties of Ni-WC Composite Coatings[J]. *Wear*, 2004, 257(1): 142-147

[14] Fernández MR, García A, Cuetos JM, *et al*. Effect of Actual WC Content on the Reciprocating Wear of a Laser Cladding NiCrBSi Alloy Reinforced with WC[J]. *Wear*, 2015, 324-325: 80-89

[15] Amado JM, Yáñez A, Tobar MJ, *et al*. Morphology and Characterization of Laser Clad Composite NiCrBSi-WC Coatings on Stainless Steel[J]. *Surf. Coat. Technol*., 2006, 200(22): 6 313-6 317

[16] Cho JE, Hwang SY, Kim KY. Corrosion Behavior of Thermal Sprayed WC Cermet Coatings Having Various Metallic Binders in Strong Acidic Environment[J]. *Surf. Coat. Technol*., 2006, 200(8): 2 653-2 662

[17] Yao SH, Su YL , Shu HY , *et al*. Corrosive Resistance of HVOF WC Coatings with a Different Binder[J]. *Key Eng. Mater*., 2017, 739:120-124

[18] Zhang Q, Lin N, He Y. Effects of Mo Additions on the Corrosion Behavior of WC-TiC-Ni Hardmetals in Acidic Solutions[J]. *Int. J. Miner. Metall. Mater*., 2013, 38(3): 15-25

[19] Sutthiruangwong S, Mori G. Corrosion Properties of Co-based Cemented Carbides in Acidic Solutions[J]. *Int. J. Miner. Metall. Mater*., 2003, 21(3-4): 135-145

[20] Fan L, Chen HY, Dong YH, *et al*. Wear and Corrosion Resistance of Laser-cladded Fe-based Composite Coatings on AISI 4130 Steel[J]. *Int. J. Miner. Metall. Mater*., 2018, 25(6): 716-728

[21] Davoodi A, Pakshir M, Babaiee M, *et al*. A Comparative H_2S Corrosion Study of 304L and 316L Stainless Steels in Acidic Media[J]. *Corros. Sci*., 2011, 53(1): 399-408